A Device to Study the Initiation and Propagation of Calcium Transients in Cultured Neurons after Mechanical Stretch

THERESA A. LUSARDI,[1] JEFF RANGAN,[1] DAVID SUN,[1] DOUGLAS H. SMITH,[2] and DAVID F. MEANEY[1]

[1]Department of Bioengineering, University of Pennsylvania, Philadelphia, PA and [2]Department of Neurosurgery, University of Pennsylvania, Philadelphia, PA

Abstract—The brain is generally considered protected from mechanical forces. However, during traumatic events, cells in brain tissue are exposed to complex mechanical events including transient acceleration, pressure, and direct stretch. This paper presents a model to expose cultured cells of the central nervous system (CNS) to a defined stretch insult. The system is designed to apply a single transient uniaxial stretch to cultured cells; control of both the magnitude and rate of stretch allows study of a broad range of conditions, from physiologic to traumatic. Distinct from previous cell-stretching systems, we control the fraction of cells deformed and examine the response of stretched cells or the surrounding population of unstretched cells, the "mechanical penumbra," of the same culture. Finally, we use this new model with cultured neurons, measuring the acute calcium response in traumatically stretched cells and the propagation of this calcium influx in neighboring, but unstretched cells. Stretched neurons exhibit a strain rate and magnitude-dependent response, unstretched exhibit an "all-or-none" response. This model will further our understanding of the complex interaction between mechanical stimuli, resulting biochemical cascades, and interaction between mechanical and other challenges, thereby furthering our understanding of the initiation and evolution of cellular damage following traumatic CNS injury.

Keywords—CNS trauma, *In vitro* model, Fura-2.

INTRODUCTION

Mechanical forces on cells are one of the many signals that can direct and modulate cell structure and function. An increasing amount of knowledge across many cell types demonstrates that mechanical signals can trigger both short- and long-term changes in cell function and structure; examples include long-term adaptation of the cell cytoskeleton and temporal changes in gene expression.[3,4,17,18,26]

In the central nervous system (CNS), cells can experience a broad range of mechanical forces spanning from normal physiological motions to traumatic injury. For example, estimates of tissue strains in the spinal cord during normal neck flexion-extension show that segments of the cord deform less than 7–8% in approximately 2–3 s.[46] In comparison, physical model tests and finite element simulations of the brain motion during impact loading show that tissue deformations during impact are applied very rapidly—typically less than 50 ms in duration—and can exceed 25% in some brain regions.[23,24,34,47] The deformation patterns throughout the brain during impact vary spatially, and it is common to observe predicted areas of high deformation adjacent to regions experiencing little or no deformation. Most investigators have associated these areas of high deformation with injury to the tissue, and have focused their efforts on understanding the molecular progression of events that occur in these regions following traumatic injury. Previous work *in vitro* has shown rapid deformations applied to neurons and astrocytes cause immediate changes in the resting membrane potential,[39] are associated with a calcium influx,[12,20,35,43] and can initiate immediate changes in cell morphology.[9,10,38,44]

Currently unknown is how mechanical deformations of cells in the CNS can trigger changes in adjacent, *unstretched* cells within the tissue. This is an area of investigation akin to studies of anoxic/ischemic injury to CNS tissue, where the adjacent tissue penumbra surrounding the infarct region has been a major target of pharmacotherapy.[15] Hypotheses about the mode of propagation of a targeted insult include the release of glutamate, nitric oxide, potassium, and free radicals, many of which act as feedback control over one another.[2,8,32,33,45] In turn, we propose that there may be a "mechanical penumbra" surrounding the areas that are deformed directly during CNS trauma. The propagation of biochemical changes to the undeformed regions could alter the function of cells in a strain-independent manner. Accordingly, as with the penumbra in anoxic/ischemic injury, the mechanical penumbra may represent a significant therapeutic target for improving function after traumatic CNS injury.

In this report, we present a technique to examine the response of cultured neurons to a direct stretch, as well as

Address correspondence to David F. Meaney, PhD, Associate Professor of Bioengineering, Department of Bioengineering, University of Pennsylvania, 3320 Smith Walk, Philadelphia, PA 19104-6392. Electronic mail: dmeaney@seas.upenn.edu

the response of adjacent unstretched cells following stretch. We use finite element modeling to examine the range of possible strain conditions that we can apply with our device. We characterize the strain field applied to cultured neurons, ensure that this deformation does not propagate to the adjacent neuronal population, and show that a single mechanical stretch stimulus can initiate changes in cytosolic calcium in the mechanical penumbra region. We view this as a first step in developing a more complete understanding of how mechanical deformations can trigger changes in cells of the CNS under conditions that approximate mechanical injury, providing new insights into therapeutic strategies for treating the injured nervous system after traumatic insults.

MATERIALS AND METHODS

System Overview

The device is a microscope-mounted system that allows cultures to be viewed using phase microscopy or standard fluorescence imaging techniques. Cells are plated on a flexible elastic substrate attached to a stainless steel well, and a cover plate is attached over the stainless steel well to form a closed chamber containing the cultured cells, supporting media, and the elastic substrate [Fig. 1(A)]. A pneumatic pressure pulse applied to the chamber causes the elastic substrate to deflect and, in turn, stretch the cultured cells [(Fig. 1(B)]. A stainless steel plate placed underneath the elastic substrate controls the portion of the substrate permitted to deflect downward during the chamber pressurization. By altering the geometry of the material removed from the underlying rigid support plate, one can control both the relative fraction of the cell population experiencing the applied stretch (specified by the area of the removed material divided by the original culture area), as well as the anisotropy of deformation field applied to cultured cells in the stretched region (determined from the geometry of the section of material removed from the plate). A fused silica window (Esco Products Inc., Oak Ridge, NJ) was incorporated into the stainless steel plate to allow microscopic observation of the unstretched portion of the culture. "Sham" experiments were performed by replacing the entire stainless steel plate with a fused silica plate and exposing the cells to transient pressure with no substrate deformation. "Control" experiments were also conducted, where the cell cultures were placed on the microscope stage but received no pressure or substrate deformation. Injury parameters were controlled and monitored for each experiment using a custom data acquisition system. Substrate deformation was directly proportional to the pressure input to the system, and set by a two-stage regulator attached to a tank of compressed medical grade air (BOC Gasses, Lebanon, NJ). Pressure input could be controlled to target the substrate deformation to within 0.05, or 5% stretch. The chamber pressure was controlled by a solenoid (Parker General Valve, Fairfield, NJ).

Open time for the solenoid was operator controlled from 20.5 to 1354 ms. Chamber pressure was monitored using a dynamic pressure transducer (Entran, Fairfield, NJ), allowing confirmation of the magnitude, duration, and recovery of the chamber air pressure. Adjustments to the system compliance were made such that all onset times (20.5, 205, and 1354 ms) shared the characteristic linear onset and exponential decay shown in Fig. 1(B) for the 20.5 ms onset deformation.

Predicting Mechanical Response of Substrate

Finite element simulations were used to examine the strain field produced in the substrate with different plate geometries. The strain field resulting from a circular area of elastic membrane exposed to a pneumatic pressure is well characterized.[25] We studied the less commonly used rectangular membrane geometry, which can provide a range of different local strain fields in the membrane based on the ratio of the length (L) of the membrane relative to its width (W). Specifically, we were interested in producing a "constrained uniaxial" deformation, where the membrane deformation was much larger in one direction than the transverse direction ($E_{xx}/E_{yy} \gg 1.0$). A commercially available finite element package (ABAQUS/Explicit, Hibbit, Karlson, and Sorenson, Inc., Pawtucket, RI) was used to generate a finite element mesh of several different rectangular geometries to encompass the range of geometries that could be used in the experimental studies. Symmetry allowed modeling of one-fourth of the rectangular region; the top and right edges were modeled with a supported boundary condition, and the bottom and left edges of the membrane as axes of symmetry. Shell elements with a finite thickness were used in all simulations. Pressure loading was applied to the top surface of the mesh, and a range of pressure loading conditions was examined to define relationships between the applied pressure (P) and both the peak membrane displacement at the center of the membrane (δ) and regional substrate strain [$E_{xx}(x, y)$, $E_{yy}(x, y)$] that occurred across the membrane. Mesh refinement studies were performed to ensure mesh convergence across the range of simulations conducted. A final mesh resolution of 0.02 mm was used in all simulations.

The membrane material properties used in the finite element simulations were derived from testing of silastic membrane specimens (Specialty Manufacturing, Saginaw, MI) under uniaxial loading in an Instron electromechanical testing machine (Model 4206, Canton, MA). Membrane samples ($n = 7$ samples; each sample 127-μm thick) were prepared using a typical hourglass test geometry, with the width (1.27 mm) and the length (5.46 mm) of the narrow region held constant across samples. Samples were attached to the testing machine using standard pneumatic grips, and marks were placed on the material at the grip points to examine for possible slip of the material at the grips during
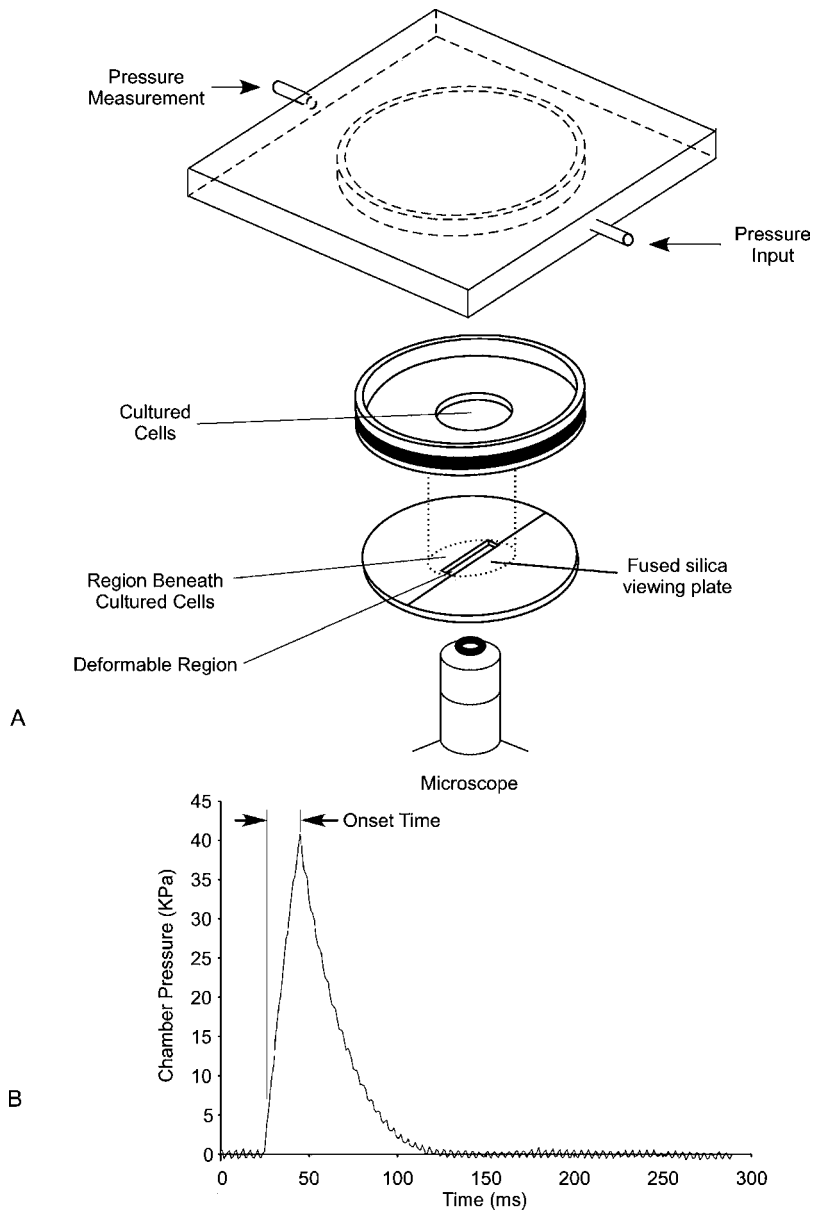
FIGURE 1. Cell stretch device. An exploded view of the device components (A). The top plate screws directly to the microscope stage (not shown), forming a sealed chamber. A fused silica window allows the imaging of cells adjacent to the region of stretch. The transient chamber pressure is measured directly for each experiment, as shown in (B).

the stress–strain test. A ramp-loading profile (2.54 mm/min) was used to stretch the specimens until failure, and the force was recorded (5 Hz sampling rate) during the testing period. Cauchy stress–stretch ($\sigma - \lambda$) relationships for the membrane were computed from the measured force (F), original cross-sectional area (A_o), initial specimen length (L_o), and the applied displacement occurring in each test (δ):

$$\sigma = \frac{F}{A_o} \qquad (1)$$

$$\lambda = \frac{L_o + \delta}{L_o} \qquad (2)$$

An incompressible first-order Ogden hyperelastic material[29] was used to model the behavior of the membrane during uniaxial loading:

$$\sigma = \frac{2\mu}{\alpha}(\lambda^{\alpha-1} - \lambda^{-\alpha/2-1}), \qquad (3)$$

where α and μ (Pa) represent the material constants of the Ogden material, λ is the stretch ratio along the axis of elongation, and σ is the Cauchy stress in the material. Parameters for the Ogden material descriptions were computed using a least-squares-minimization procedure

(IgorPro, Wavemetrics, Inc., Lake Oswego, OR, USA) that best fit the experimental stress–stretch data.

Using the measured material properties, finite element simulations were conducted to examine (a) the response of the membrane to dynamic pressure loading, (b) the potential change in membrane displacement as the rate of pressure loading was changed, and (c) the variation in the strain field along the surface of the membrane as the geometry was changed from square ($L/W = 1.0$) to increasingly narrower rectangular shapes ($L/W = 24$).

Verifying Predictions of Membrane Mechanical Response to Pressure

To confirm the predictions from the finite element simulations, measurements of the centerpoint vertical displacement of the membrane were made in response to an applied pressure loading. For these measurements, one membrane geometry ($L/W = 12$) was examined and a rigid plate with a rectangular slit (18 mm × 1.5 mm) removed was placed underneath the elastic substrate. Once positioned on the microscope stage, the membrane ($n = 7$ samples total) was inflated to a static position and held at a constant pressure. The z position of the microscope stage was adjusted to focus on the membrane in both the undeformed and inflated positions; the net z movement of the stage was used as a measure of the peak centerline displacement of the membrane to the static pressure. For each membrane sample, seven separate pressures were used to develop a measure of the pressure–centerline deflection curve over the range of pressures used in the experimental condition.

In addition to verifying pressure-displacement predictions, measurements of the membrane strain field were completed by tracking the displacement of fluorescent microspheres attached to the membrane surface during a range of static inflation conditions.[12] We report substrate strain, rather than cell strain, because of the difficulty quantifying the cell strain using fluorescent beads (1-μm diameter) that are similar in size to the cultured cells (10 μm in diameter), a situation that could create substantial error in the calculation of strain locally on the cell surface. Silastic membranes coated with poly L-lysine (PLL) as for primary cell plating (see below) were incubated in a saline solution containing a 1:100 dilution of microspheres (nominally 1-μm diameter, Molecular Probes, Eugene, OR) and incubated for 10 min. Following incubation, membranes were rinsed twice to eliminate beads in solution, but not attached to the substrate. Digital images (1280 × 1024) of the beads attached to the membrane were taken using a DXM-1200 (Nikon Inc., Tokyo, Japan), with a 40 × objective plus an additional 2 × magnification from the Multi-Image-Module (Nikon). All bead experiments were done with 50-μm-thick membranes and a 1.5-mm-slit plate in place. Images were analyzed with Scion Image (Frederick, MD), which reported the centroid of each microsphere, excluding clusters

of microspheres. Beads in the inflated membrane region, as well as the adjacent region of membrane supported by a fused silica plate, were tracked under the inflation pressures used in the cell culture experiments.

A bead pair was tracked to determine the initial segment length (dS_o) and final segment length (dS_f) between the beads. A triad of beads, forming three separate line segments covering a triangular region on the silastic membrane, was tracked to develop measures of the difference in line segment lengths ($(dS_f^2 - dS_o^2)_i$; $i = 1, 2, 3$) for three bead pairs. In this analysis, we did not explicitly account for the potential out of plane bead displacement that occurs when the membrane is inflated to its semicircular shape. However, after analyzing the radius of curvature for the largest deformation (50%) and using typical segment lengths (>100-pixels long), we concluded that the error in substrate strain measurement from omitting the out of plane displacement was less than 0.2%, within the range of error from other sources. The Green's strain tensor (E_{ij}) was calculated from the following system of equations:

$$\left(dS_f^2 - dS_o^2\right)_i = 2\left(E_{xx}\Delta x_i^2 + 2E_{xy}\Delta x_i \Delta y_i + E_{yy}\Delta y_i^2\right)$$
$$i = 1, 2, 3$$

where Δx_i and Δy_i represent the difference in the x and y coordinates of the beads for line segment i of the initial bead pairs. To minimize quantization error in the calculation of strain, triangles with line segments less than 100-pixels long, areas less than 500 square pixels, or containing angles less than 6° were excluded from analysis.

Examining the Response of Cultured Neurons to Mechanical Stretch

All procedures involving animal use were approved by the Institutional Animal Care and Use Committee at the University of Pennsylvania. We used two separate culture components—a neuronal (silastic) culture and a separate glia-rich "support" co-culture—to produce a nearly pure neuronal culture attached to a flexible, elastic membrane. Primary hippocampal neuronal cells were isolated from E17-E19 Sprague-Dawley rats (Charles River, Wilmington, MA). Isolated hippocampi were incubated in trypsin/DNAse (Roche Applied Science, Indianapolis, IN) solution for 20 min at 37°C, 5% CO_2, and then triturated in a 10-ml pipette after adding soybean trypsin inhibitor (Gibco, Carlsbad, CA). Cells were centrifuged for 5 min at 1000 RPM and resuspended in 10 ml of Neurobasal media (Gibco) supplemented with 2% B-27 (Gibco), 0.5 mM L-glutamine (L-gln, Gibco), 25 μM L-glutamate (L-glu, Sigma, St. Louis, MO), and 1% Pen/Strep (Gibco), and filtered serially through Nitex mesh (Cross Wire Cloth, Bellmawr, NJ). Hippocampal cell suspensions were diluted and plated in plating media consisting of Neurobasal media supplemented with 2% B-27, 0.5 mM L-glu, 25 μM L-gln, 1% Pen/Strep, and 5% FBS (Hyclone, Logan, UT).

Cells were plated at 750,000 cells/ml (0.5 ml/well) onto thin, clear, flexible elastic membranes (silastic, Specialty Manufacturing, Saginaw, MI) coated with 1 μg/cm^2 PLL (Sigma) and 1 μg/ml laminin (Collaborative Biomedical, Bedford, MA). At 3 h *in vitro*, all cells from the plating process were fed again with the plating media. Following feeding, support cultures that were composed primarily of glial cells were placed above the silastic cultures without damaging the freshly isolated cells. These support cultures were prepared a week prior to plating of the silastic cultures, and were plated initially at 500,000 cells/ml onto matrigel (1:8 dilution in ddH$_2$O, Collaborative Biomedical) treated 12 mm millicell wells (Millipore, Bedford, MA); support cultures were not treated with mitotic inhibitors, resulting in a glial-cell-rich culture. Once placed above the hippocampal culture, the support culture received the same feeding and media as the silastic culture. The silastic and support cultures were fed at 4 and 7 DIV with Neurobasal media supplemented with B-27, L-gln, and 5% FBS. Cultures were treated with a mitotic inhibitor (5 μM cytosine β-d-arabinofuranoside, Sigma) for 24 h starting at 4 DIV. Prior to conducting an experiment, the overlying support culture was removed from the culture well, leaving cells that were well attached to the silastic membrane. All experiments were performed with 10- or 11-day-old silastic cultures. With this plating procedure, the silastic cultures at 10 or 11 DIV consisted of 91 $\pm$ 3.3% neurons, measured as the fraction of type-III beta tubulin positive cells with respect to all nuclei labeled with Hoechst (Molecular Probes). Cytosolic calcium levels were measured in the silastic cultures after stretch using the ratioable fluorescent calcium dye fura-2AM (Molecular Probes, Eugene, OR). Fura-2 is a calcium chelator with k_d = 224 nM,[14] making it most sensitive at physiologic levels of calcium. Cultures were loaded at 37°C for 45 min with 5 μM fura-2, rinsed, and then allowed to sit for 10 min in CSS (120 mM NaCl, 5.4 mM KCl, 0.8 mM MgCl$_2$, 1.8 mM CaCl$_2$, 25 mM HEPES, 15 mM glucose, pH = 7.4, osmolarity adjusted to 330 mOsm with sorbitol). MetaFluor (Universal Imaging, Downingtown, PA) software was used for all image capture and analysis. Images were captured using an intensified 8-bit Hamamatsu CCD (Optical Apparatus, Ardmore, PA). The excitation shutter and filter wheel were controlled using a Lambda 10-2 (Sutter Instruments, Novato, CA). Fluorescence ratio images (F$_{340}$/F$_{380}$, 510-nm emission) were captured at 2-s intervals for 1 min prior to stimulus; capture continued for 5 min at 2-s intervals following the stimulus.

To analyze the fura-2 fluorescence data, individual cells were first identified using available software, tracked over the recording time of the experiment, and the maximum fura-2 ratio was calculated for each cell in the field of view. To avoid the displacement gradient near the edge of the deformed region, cells located only in the center region of the membrane were used for analysis. To present the response of the entire cell population, the peak fura-2 ratio information was presented using cumulative frequency plots. With this plot format, the relative fraction of cells that showed a peak ratio less than a given value could be read directly. Moreover, the shift in the response of the cell population under different experimental conditions could be viewed directly by the shape of the cumulative frequency plots.

STATISTICS

For calcium imaging of mechanically injured neurons, a minimum of three separate culture wells were used for each experimental group studied, with an average of 50 $\pm$ 20 cells analyzed per culture well. To avoid cell isolation bias, cultures used for each experimental group were spread across a minimum of two separate cell isolations. An initial statistical analysis using a nested design showed that neither cell isolation nor well ID were significant factors in the analysis, and therefore data within each experimental group was grouped accordingly. Statistical analyses were performed using SAS V.8 (Cary, NC). Since the peak calcium levels varied over three orders of magnitude, the fura-2 ratio data were analyzed using a generalized linear model with a log link function; the natural log of the mean of the data was modeled as a linear function of the factors.[21] The variance at any combination of main effects (strain, onset, treatment, and region) was modeled as the square of the mean of the data. Wald tests were used to determine significant differences between specific combinations of factors. A Bonferroni correction was used to adjust for multiple comparisons.[19]

RESULTS

Anisotropy of Substrate Strain Field Is Adjustable through Membrane Geometry

Across different membrane geometries, the strain field predicted from finite element simulations at the center of the membrane changed from an equibiaxial field (square geometry) to a strain field that was aligned principally along one axis of the membrane (Fig. 2). Although the square geometry produced a membrane deformation field that was equibiaxial at the centerpoint of the membrane ($E_{yy}/E_{xx} = 1$), the membrane strain quickly became nonuniform beyond the membrane center. For narrow membrane geometries, a much larger deformation was produced across the width of the slit (E_{xx}) in comparison to the deformation along the slit length (E_{yy}). Beyond geometries where the length was approximately 8 times the width of the membrane, the deformation field was principally uniaxial ($E_{yy}/E_{xx} < 0.001$). We chose to study this uniaxial deformation field in more detail, and selected a long, narrow geometry ($L/W = 12.0$) that produced a highly anisotropic strain field ($E_{yy}/E_{xx} < 10^{-2}$) for subsequent experiments and simulations. In all membrane simulations with this geometry, the mesh was
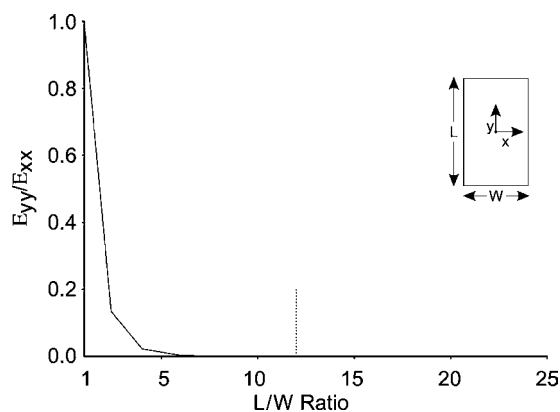
FIGURE 2. Anisotropy of the strain field at the center of the membrane surface is dependent on the membrane geometry. For a square geometry, the ratio of substrate strains at the center of the membrane is 1.0. In comparison, narrow membrane geometries (*L/W* > 8.0) produced a uniaxial deformation field at the center of the membrane ($E_{yy}/E_{xx} < .001$). The dotted line represents *L/W* = 12, the ratio used for subsequent testing with cultured neurons.

successively refined to achieve numerical convergence, and each thickness simulation was run separately. Acceptable mesh convergence and model stability was achieved when the refined mesh predicted a centerline membrane displacement less than 0.1% different from the previous mesh, and when the deformed mesh contained no significant element warpage or high artificial strain energy. The simulations used in this study satisfied these criteria, across the different membrane thicknesses, material properties, and pressurizations simulated in the study.

Predicted Membrane Displacement Corresponds with Measured Displacement Response

For the chosen narrow membrane geometry (*L/W* = 12), both the measured and predicted vertical (*Z*) displacement of the membrane were directly proportional to the applied pressure. Parametric analysis of the measured material properties (μ, α, and t) showed that the strain and displacement predictions were sensitive only to the prestressed membrane thickness. Once prestressed (10%), the nominally 50-μm-thick silastic membranes ranged in thickness from 18 to 30 μm. Accordingly, finite element simulations were run at these extremes [dashed lines, Fig. 3(A)]. Using the measured material properties for the silastic membrane ($\mu = 660$ kPa; $\alpha = 2.81$), we found that predictions from a finite element model of the membrane geometry corresponded with the static pressure–centerpoint deflection relationship measured for a series of membrane samples [Fig. 3(A)]. We found no difference in the predicted displacement when we used different pressure onset rates from 20 to 100 ms, and therefore feel that the static measurements may be reasonable estimates of the dynamic membrane motion. Peak predicted centerpoint displacement at

a given pressure was most sensitive to initial membrane thickness, changing the predicted displacement by approximately 25% for thinner membranes (50 μm) used to study larger substrate stretch conditions. At low pressures, measures were within 6% of predicted values, increasing to 11% at 45 KPa. For all membranes, the vertical displacement was maximum along the centerline and decreased to zero at the fixed periphery [Fig. 3(B) and (C)]. However, the change in vertical displacement was gradual along the width of the membrane (*x*), decreasing to 79% of its peak centerline value halfway between the centerline and the membrane edge [Fig. 3(B)]. Along the length of the membrane (*y*), the vertical displacement was constant along the middle 72% of the membrane, and then rapidly decreased to zero at the edge [Fig. 3(C)].

Measured membrane strains corresponded to predicted strains, and were principally directed along the width of the membrane region. Using the displacement of beads attached to the surface of the membrane before and during pressurization, a linear relationship between the measured and predicted strains was measured [$R^2 = 0.995$, Fig. 4(A); $(E_{xx})_{\text{measured}} = 0.91 \times (E_{xx})_{\text{predicted}}$]. Beyond a membrane strain of 0.5, the statically inflated membranes would rupture and prevent an experimental verification of the predicted deformations from the FEM. Therefore, the data from these cell culture experiments at these pressurization levels were reported as ">50%." The minor principal strains computed from the bead displacements across different pressures was significantly less than the major principal strains ($p < .001$), consistent with predicted behavior. Across the membrane surface, the maximum principal strain (E_{xx}) predicted by the FEM was uniform across the width of the slit [Fig. 4(B)] and across 70% of the length [Fig. 4(C)], decreasing only near the top membrane edge (normalized *Y* position = 1.0). Although the strain in the *y*-axis (E_{yy}) was markedly less than the maximum principal strain, the strain in this direction increased significantly near the top clamped edge [Fig. 4(D)]. Along the *x*-axis, E_{yy} was negligible, and not shown.

The Region Adjacent to the Deformed Membrane Area Does not Stretch

Across the range of inflation pressures used in experimental studies, there was no detectable displacement or deformation of the membrane in the region adjacent to the stretched membrane area (Fig. 5). Fluorescent beads allowed to attach to the membrane and photographed both before and during a static inflation using typical experimental pressures showed no detectable displacement compared to sham (no pressure) controls. In addition, the major principal strains measured from bead triads in the regions adjacent to the stretched membrane region were significantly different ($p < .001$) from the stretched region; across all substrate stretch conditions, the deformations measured by the bead
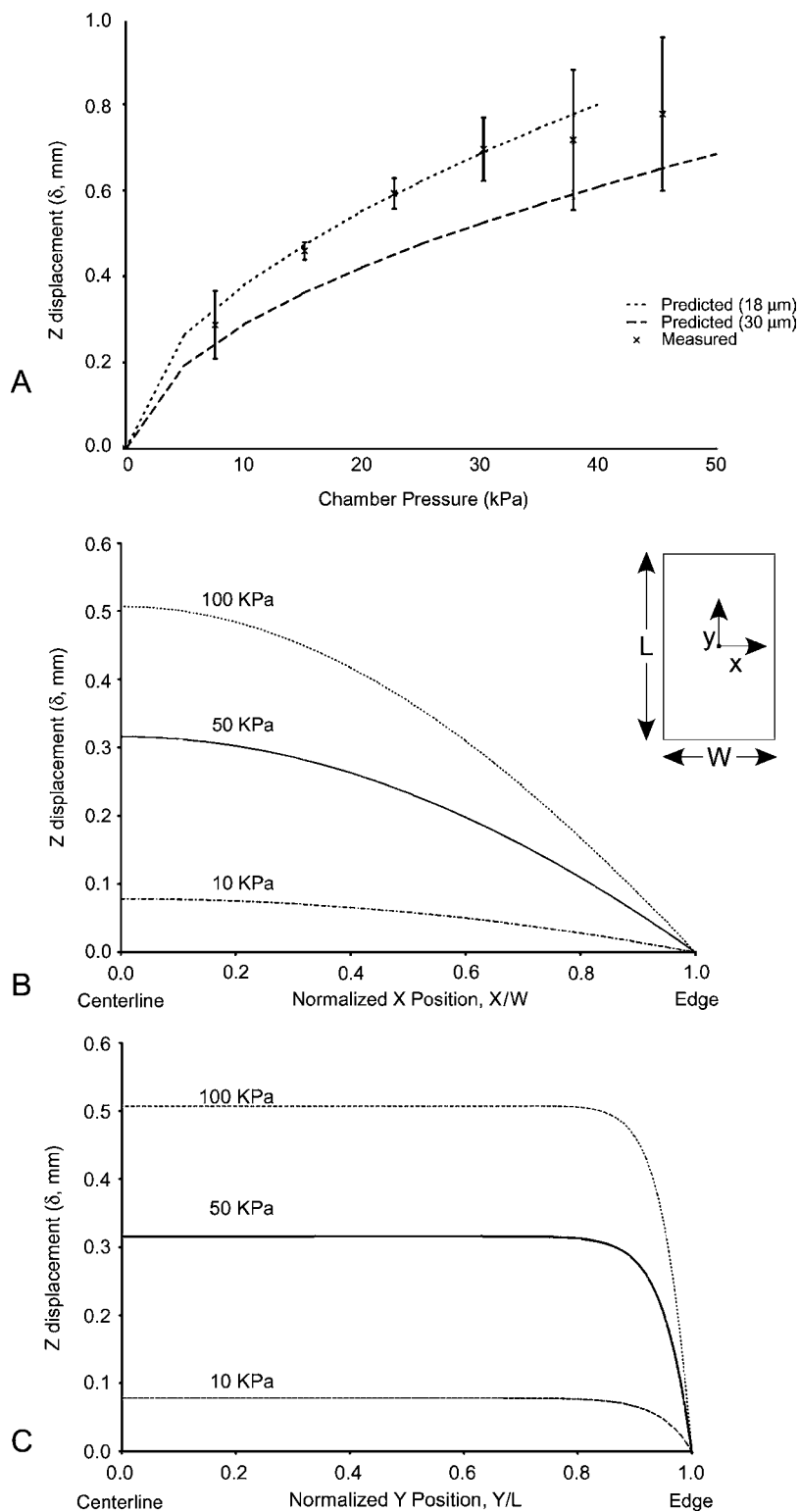
FIGURE 3. Measured and predicted membrane displacements. (A). Calculations (dashed lines) and measurements (symbols) of the centerline displacements were made for the range of membrane thicknesses available for testing (18–30 μm). Measurements fell within the range of predicted displacements over the range of pressures examined. (B). Finite element model predictions of the membrane deflection (δ) across the width (X) of the membrane showed a gradually decreasing vertical (Z) displacement from the membrane centerpoint. (C). The vertical (Z) deflection along the length of the membrane (Y) is constant along most of the surface. *Note*: In (B) and (C), 0 represents the free centerline edge, and 1 the clamped edge.
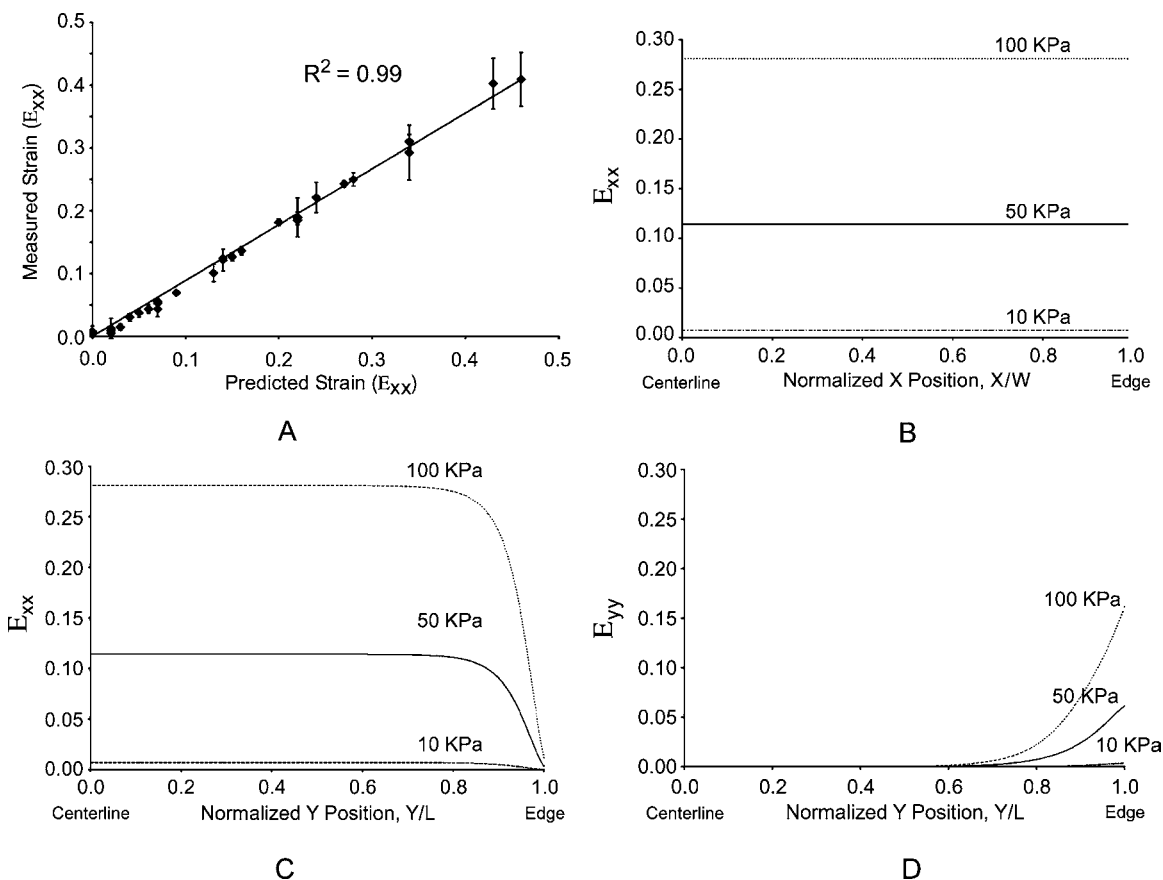
FIGURE 4. Comparison of measured and predicted membrane deformations. (A). The relative displacements of beads placed on the membrane surface were used to measure deformations in the membrane during inflation. Measured deformations in the central region of the membrane correlated to the predicted membrane deformations in the same region. [(E_{xx})$_{meas}$ = 0.91 (E_{xx})$_{pred}$; R^2 = 0.995) (B–D). Membrane strain profiles across the membrane surface for a FE model using a narrow geometry (L/W = 12). The largest strain component, E_{xx}, is uniform across the width (B) and across most of the length (C). The strain component in the y direction (E_{yy}) is negligible along the width of the slit (not shown), and considerably less than E_{xx} along the length of the slit (D), with the exception of the clamped edge effects (near Y = 1).

triads in the remote region was less than 1%, within the precision of the strain measurement of the technique.

Hippocampal Neurons Show an Immediate Increase in Cytosolic Calcium after Stretch

Similar to previous reports, the increase in cytosolic calcium caused by a single mechanical stretch was dependent upon both the rate and magnitude of applied deformation (Fig. 6). Neurons were plated uniformly on the silastic. The periphery of the slit was avoided for analysis due to the reduced uniformity of the strain field predicted by the finite element simulations. Typically, the neurons would show an immediate increase in the fura-2 ratio that would slowly return toward prestretch values over the 5-min monitoring period [Fig. 6(A)]. At no time did the cells detach from the membrane following stretch injury. For stretch onset times that simulated mechanical injury (20.5 ms), a single membrane stretch insult was sufficient to cause a signifi-

cant increase in cytosolic calcium across the cell population [Fig. 6(B)]. Although the peak fluorescent response for individual cells in the population spanned a broad range, the average cell response increased in proportion to the applied substrate stretch ($p < 0.001$). Data is presented as the cumulative fraction of cells responding at or below a given fura-2 ratio. Half of the neurons responded below the reported median, half above the median. For a substrate strain of 3–6%, the median value of the peak fura-2 ratio measured across cells in this group was 2.86; the median value increased to 9.32 at a substrate strain of 12–17%, and increased further to 15.84 for cells exposed to strain >50% [Fig. 6(B)]. Using a subsequent ANOVA analysis, we determined that cell populations subject to dynamic pressure loading but no deformation (sham experiments), cytosolic calcium was not significantly increased [median of 0.48, Fig. 6(B)] compared to control experiments (data not shown). For the highest strain group (>50%), we examined the rate dependence of the peak calcium response
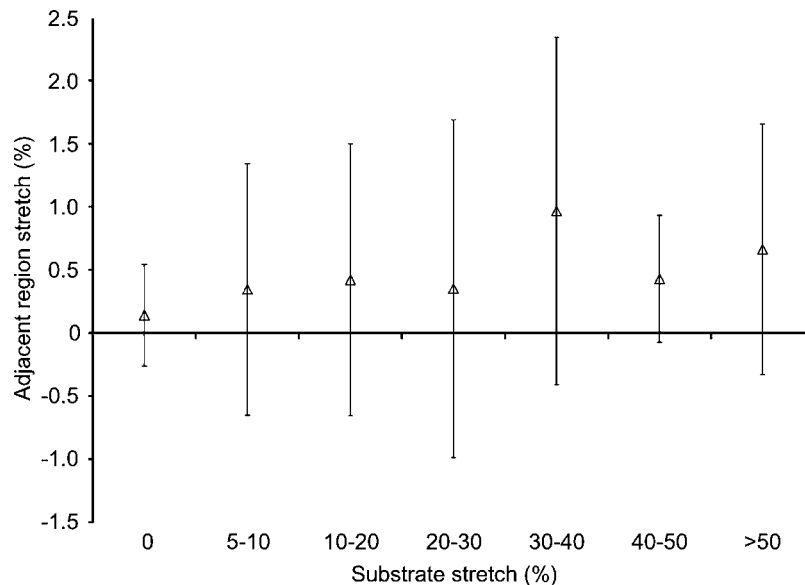
FIGURE 5. Motion and deformation of the silastic membrane region adjacent to the deformed area following a pressurization. The region analyzed was supported by a fused silica plate, and was adjacent to the unsupported membrane region that was deformed by the pressurization. Several stretch conditions were studied, encompassing the range of substrate stretch conditions used in the cell culture studies. Analysis of bead triads in the adjacent region showed no significant membrane deformation occurred in this area, despite having significant substrate stretch levels in the deformed membrane regions.

[Fig. 6(C)], finding a significant effect with respect to the onset time ($p < 0.001$). We measured a decrease in the median response from 15.84 for 20.5-ms onset to 14.09 for 205-ms onset, and to 3.78 for an onset of 1354 ms.

In the adjacent population of unstretched cells, cytosolic calcium changes were observed for all substrate strains (Fig. 7). Peak changes in $[Ca^{2+}]_i$ in the penumbra region were much lower than the levels measured in the stretched cells. We do not attribute this decrease to a problem in light transmission through the fused silica plate, since NMDA agonist stimulation of penumbral neurons produced the same relative change in fluorescence ratio whether the fused silica plate was in the light path or not. Additionally, the average remote response did not increase significantly in proportion to the applied substrate strain. While the average fura-2 response in the remote region increased significantly over the sham and control values ($p < 0.01$), the increases were in an "all-or-none" manner, and not significantly different from one another. The fura-2 ratios increased slightly with stretch level, with median responses of 1.31, 1.87, and 2.48 associated with strains of 3–6%, 12–17%, and >50%, respectively.

DISCUSSION

Previous investigations of the biomechanics of nonpenetrating CNS trauma have studied the response of nervous tissue to the mechanical loading that occurs during trauma, with the goal of understanding as to how the mechanical energy translates to tissue damage following impact. As an extension to this previous work, we and other groups are now examining the neuronal response to rapid deformations at the cellular level. With these *in vitro*-based models, one can address three main areas of research: the mechanical–biological coupling process in neurons, the biological events triggered by mechanical strain and their differences from chemical stimulation in neurons, and the propagation of biochemical signals from cells in mechanically injured tissue into undeformed regions. The model presented in this study simulates a range of deformations that occur in the central nervous system, from physiologic to traumatic. Data is presented to show that the acute calcium transient resulting from mechanical stimulations across this spectrum can vary considerably. We show that cultured neurons are sensitive to both absolute strain and the time over which it is applied, and that the stretch-induced calcium transient propagates to cells in the "mechanical penumbra" in a stretch-independent manner.

The direct cellular deformation that occurs as brain tissue is traumatically deformed locally and is a widely studied physical stimulus to the nervous system. Using a stylus or other instrument to denude or "scratch" away portions of the cell population represents a highly localized and severe cellular deformation, and one can therefore examine the propagation of injury from lacerated tissue.[6,18] However, such tissue tearing is rare except for instances of penetrating injury or severe levels of nonpenetrating injury, and is typically localized in white matter tracts.[36] As such, devices to stretch cells below their structural failure can study a very broad spectrum of mechanical injury in the CNS. Recent
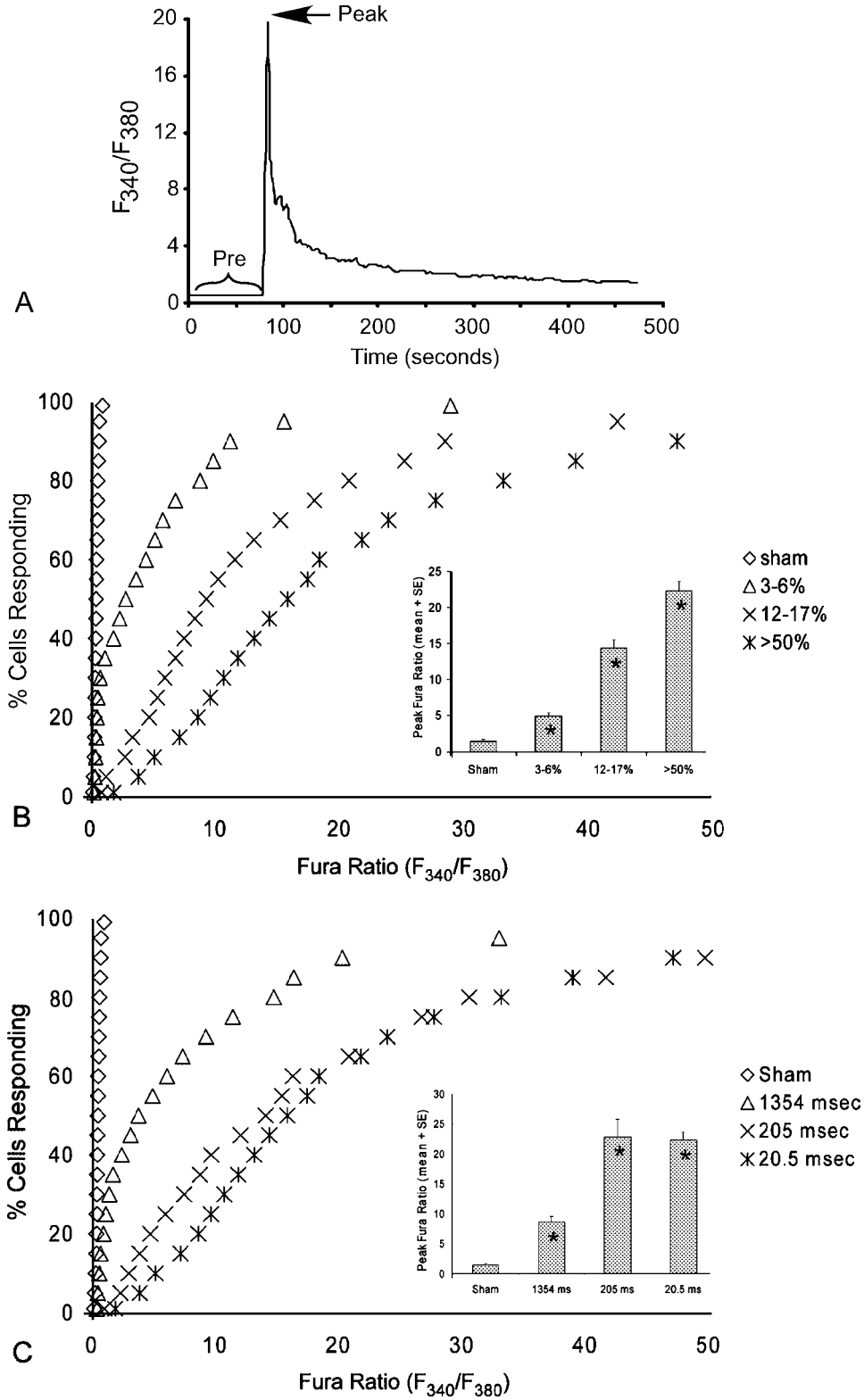
FIGURE 6. Dose response of cultured hippocampal neurons to substrate stretch. (A). Fura-2 ratio (F_{340}/F_{380}) trace for a single neuron, an indication of the cytosolic calcium concentration in the cultured neurons. (B). Using a time to peak stretch (20.5 ms) to simulate traumatic injury, the change in fluorescence ratio was clearly dependent on the level of substrate stretch, with increasing levels of stretch eliciting higher changes in the fura-2 fluorescence ratio. (C). The peak change in the fura-2 fluorescence ratio was sensitive to the onset time of applied stretch. Reducing the time to peak stretch from 1.354 s to 20.5 ms increased the median fluorescence ratio from 3.78 to 15.84. The population response is shown symbolically for each strain/onset condition, with the mean data displayed as a bar graph in the insets (B and C). *$p < 0.001$.
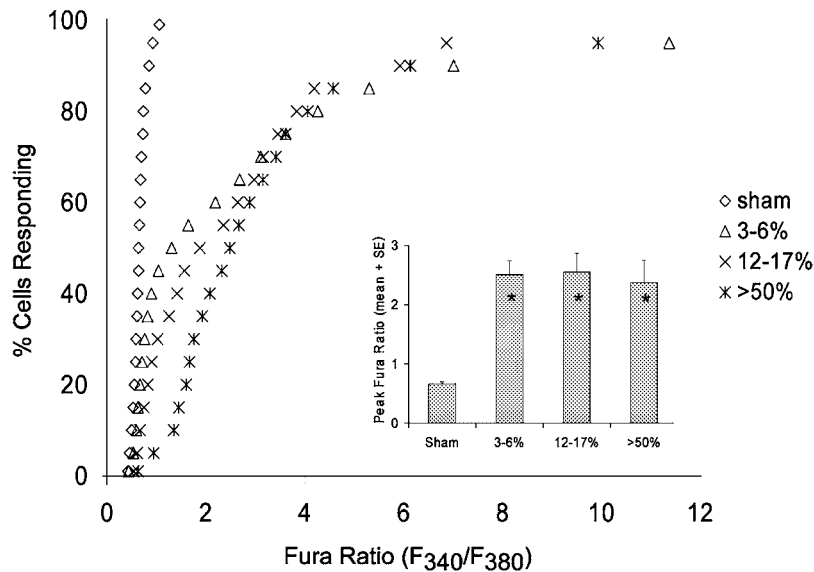
FIGURE 7. Characterization of response in unstretched substrate region adjacent to area of stretch. Although no deformation occurred in the adjacent region (see Fig. 5), neurons in this region did show a calcium increase after a stretch stimulation that was different from sham stimulation. Unlike the neurons in the stretched region (see Fig. 6), the magnitude of the calcium response did not change significantly for different levels of membrane stretch. The population response is shown symbolically for each strain, with the mean data displayed as a bar graph in the inset. *$p < 0.001$. Sham refers to the condition where pressure is applied to the cultures, but the underlying substrate is not deformed.

studies in neurons and astrocytes have demonstrated how a single mechanical stimulus can initiate early biochemical changes, a delayed membrane depolarization, and a longer term decrease in astrocytic viability.[1,11,12,35,39]

For the model presented here, we selected the substrate stretch method of deforming neurons, and optimized the geometry of the model to apply a unidirectional strain field to the cultured neurons. In addition, to apply substantial substrate deformations (>50% strain) to the cultured neurons without a corresponding large substrate deflection, we restricted the fraction of the cell population exposed to the mechanical stimulus, preventing contact of the substrate with the stationary objective or additional complicating aspects in the microscope mounted setup. The unidirectional strain field offers some unique possibilities. The brain is a very heterogeneous tissue, but has several distinct highly organized regions (hippocampus, tracts, cortex), and some less organized regions such as the thalamus. Within these structures, neurons can often appear *in vivo* as classic bipolar cells, with three morphologically and functionally distinct compartments aligned longitudinally: an axon, the cell body, and a dendritic tree. It is likely that the strain experienced by the cells in the CNS during trauma is a combination of both the local strain gradient and the local cellular architecture. The current system will allow us to focus in the future on how the cell architecture, defined either randomly or using an available micropatterning technique,[16,40] will respond to a defined directional strain insult. By modifying the geometry of the membrane regions used to stretch cultured neurons, we can examine whether there is a de-

pendence on the strain field components in the neuronal response to traumatic deformation, potentially giving insight into the strain transducers in neurons.

Both the acute pattern of tissue damage and the continued increase of lesion growth for up to 1 year posttrauma[7,13,22,37,42] have led many to examine the importance of how post-acute chemical insults can exacerbate the initial changes that occur from the mechanical forces at the time of injury. However, absent in this analysis is how mechanical forces can initiate changes in neighboring neurons, and how these initiated changes are tolerated by the neighboring neurons. *In vitro* models of targeted neuronal lysis have shown progression of neuronal death as a function of distance from the traumatized cells, linking this death to NMDA receptor activation,[27,30] and free radical generation.[31] Media from such traumatically injured cultures has also been shown to be toxic to healthy cultures via nitric oxide synthase activation.[45] We cannot discount the possible effects of neurotransmitter release causing this increase in intracellular calcium in the adjacent population, nor can we eliminate the possibility that the synaptic signaling in the network is altered to promote these changes in intracellular calcium. In the literature, there is ample evidence that another cell type in the nervous system, the astrocyte, will both release soluble ATP and transmit signaling through intercellular gap junctions to propagate self-sustaining calcium waves in culture.[5,28,41]

With this *in vitro* model, we have shown that there is indeed a transfer of the stretch-induced calcium transient in the unstretched region of cells immediately adjacent to the

stretched region. We focused only on the very short time following the stretch insult to determine if there was an immediate change in the surrounding cells. Longer monitoring times may be used in the future to determine how these shifts in intracellular calcium can persist in the unstretched neurons, leading to a possibly important pathological process that can give rise to secondary changes in this cell population. We do not mean to link the acute changes we measure in the penumbra directly to longer term changes in cell viability, but rather present this data to demonstrate the initiation of a calcium increase in the adjacent neuronal population.

In summary, we present an *in vitro* model that allows us to investigate the links between mechanical forces and the resulting biochemical dysfunction, eventually leading to studies the can evaluate the effect of therapeutic agents on both stretched cells and their unstretched neighbors in the mechanical penumbra. The system has broader implications for studying cellular mechanotransduction, since it can easily accommodate different cell culture types. Frequently, cells in different tissue do not all experience the same mechanical stimulus, and it is likely that the integrated response of the tissue is a combination of the cellular response to local mechanical forces and the overlying response of cells in adjacent regions that experience less mechanical stimulation. For example, simple compression of cartilage samples produces a remarkably heterogeneous strain field among the chondrocytes contained within the tissue. At the signal transduction level, this raises the possibility of a "signaling gradient" that is driven by the local deformation gradient imposed on the cells in the tissue. Currently, most cell stimulation systems treat the mechanical stimulus in its purest form, attempting to precisely control the uniformity of the mechanical stimulation. With this new system, one can examine the effect of dramatic deformation gradients between deformed and undeformed cell populations, measuring the mechanisms of how biochemical signals can propagate between the two populations.

With this system, we can pose rigorous questions about cellular mechanotransduction and measure biologically relevant outcomes. As we refine our measurements, we will determine whether cellular mechanotransduction is a single, graded mechanism, or more complex, with staged mechanosensors activating different biochemical responses. This will help us understand the difference between a physiologic and a pathophysiologic response, and may be key in designing effective therapy. Further, we can begin to investigate the difference between a hypoxic or chemical insult in isolation and one that follows a mechanical trauma. The ultimate measure of a treatment for traumatic head injury is cellular function; understanding the different mediators (receptor, cytoskeletal, plasma membrane, ionic homeostasis) for different traumas is crucial in designing effective treatments.

REFERENCES

[1]Ahmed, S. M., B. A. Rzigalinski, K. A. Willoughby, H. A. Sitterding, and E. F. Ellis. Stretch-induced injury alters mitochondrial membrane potential and cellular ATP in cultured astrocytes and neurons. *J. Neurochem.* 74:1951–1960, 2000.

[2]Basarsky, T. A., D. Feighan, and B. A. MacVicar. Glutamate release through volume-activated channels during spreading depression. *J. Neurosci.* 19:6439–6445, 1999.

[3]Bazan, N. G., E. B. Rodriguez de Turco, and G. Allan. Mediators of injury in neurotrauma: Intracellular signal transduction and gene expression. *J. Neurotrauma* 12:791–814, 1995.

[4]Brown, T. D. Techniques for mechanical stimulation of cells in vitro: A review. *J. Biomech.* 33:3–14, 2000.

[5]Charles, A. C., J. E. Merrill, E. R. Dirksen, and M. J. Sanderson. Intercellular signaling in glial cells: Calcium waves and oscillations in response to mechanical stimulation and glutamate. *Neuron* 6:983–992, 1991.

[6]Citron, B. A., S. X. Zhang, I. V. Smirnova, and B. W. Festoff. Apoptotic, injury-induced cell death in cultured mouse murine motor neurons. *Neurosci. Lett.* 230:25–28, 1997.

[7]Dixon, C. E., P. M. Kochanek, H. Q. Yan, J. K. Schiding, R. G. Griffith, E. Baum, D. W. Marion, and S. T. DeKosky. One-year study of spatial memory performance, brain morphology, and cholinergic markers after moderate controlled cortical impact in rats. *J. Neurotrauma* 16:109–122, 1999.

[8]Dugan, L. L., and D. W. Choi. Excitotoxicity, free radicals, and cell membrane changes. *Ann. Neurol.* 35:S17–S21, 1994.

[9]Ellis, E. F., J. S. McKinney, K. A. Willoughby, S. Liang, and J. T. Povlishock. A new model for rapid stretch-induced injury of cells in culture: Characterization of the model using astrocytes. *J. Neurotrauma* 12:325–339, 1995.

[10]Fayaz, I., and C. H. Tator. Modeling axonal injury in vitro: Injury and regeneration following acute neuritic trauma. *J. Neurosci. Methods* 102:69–79, 2000.

[11]Floyd, C. L., B. A. Rzigalinski, J. T. Weber, H. A. Sitterding, K. A. Willoughby, and E. F. Ellis. Traumatic injury of cultured astrocytes alters inositol (1,4,5)-trisphosphate-mediated signaling. *Glia* 33:12–23, 2001.

[12]Geddes, D. M., and R. S. Cargill, II. An in vitro model of neural trauma: Device characterization and calcium response to mechanical stretch. *J. Biomech. Eng.* 123:247–255, 2001.

[13]Gennarelli, T. A. Mechanisms of brain injury. *J. Emerg. Med.* 11:5–11, 1993.

[14]Grynkiewicz, G., M. Poenie, and R. Y. Tsien. A new generation of Ca^{2+} indicators with greatly improved fluorescence properties. *J. Biol. Chem.* 260:3440–3450, 1985.

[15]Heiss, W. D. Ischemic penumbra: Evidence from functional imaging in man. *J. Cereb. Blood Flow Metab.* 20:1276–1293, 2000.

[16]Ito, Y., G. Chen, and Y. Imanishi. Micropatterned immobilization of epidermal growth factor to regulate cell function. *Bioconjug. Chem.* 9:277–282, 1998.

[17]Kampfl, A., R. M. Posmantur, X. Zhao, E. Schmutzhard, G. L. Clifton, and R. L. Hayes. Mechanisms of calpain proteolysis following traumatic brain injury: Implications for pathology

and therapy: A review and update. *J. Neurotrauma* 14:121–134, 1997.

[18] Katano, H., K. Fujita, T. Kato, K. Asai, Y. Kawamura, A. Masago, and K. Yamada. A metabotropic glutamate receptor antagonist, alpha-methyl-4-carboxyphenylglycine, attenuates immediate early gene mRNA expression following traumatic injury in cultured rat cortical glial cells. *Neurosci. Lett.* 306:101–105, 2001.

[19] Kutner, M. H., C. J. Nachtscheim, W. Wasserman, and J. Neter. *Applied Linear Statistical Models*, 4th ed. Chicago: Irwin/McGraw-Hill. 1996, 1408.

[20] LaPlaca, M. C., and L. E. Thibault. Dynamic mechanical deformation of neurons triggers an acute calcium response and cell injury involving the *N*-Methyl-D-Aspartate glutamate receptor. *J. Neurosci. Res.* 52:220–229, 1998.

[21] McCulloch, C. E., and S. R. Searle. *Generalized, Linear, And Mixed Models* (Wiley series in probability and statistics. Applied probability and statistics). New York: Wiley, 2001, xxi, 325 p.

[22] McIntosh, T. K., D. H. Smith, D. F. Meaney, M. J. Kotapka, T. A. Gennarelli, and D. I. Graham. Neuropathological sequelae of traumatic brain injury: Relationship to neurochemical and biomechanical mechanisms. *Lab. Invest.* 74:315–342, 1996.

[23] Meaney, D. F., D. H. Smith, D. I. Shreiber, A. C. Bain, R. T. Miller, D. T. Ross, and T. A. Gennarelli. Biomechanical analysis of experimental diffuse axonal injury. *J. Neurotrauma* 12:689–694, 1995.

[24] Miller, R. T., S. S. Margulies, M. Leoni, M. Nonaka, X. Chen, D. H. Smith, and D. F. Meaney. Finite element modeling approaches for predicting injury in an experimental model of severe diffuse axonal injury. In: Forty-Second Stapp Car Crash Conference. Warrendale, PA: Society of Automotive Engineers, 1998.

[25] Morrison, B., III, D. F. Meaney, and T. K. McIntosh. Mechanical characterization of an in vitro device designed to quantitatively injure living brain tissue. *Ann. Biomed. Eng.* 26:381–390, 1998.

[26] Morrison, B., III, K. E. Saatman, D. F. Meaney, and T. K. McIntosh. In vitro central nervous system models of mechanically induced trauma: A review. *J. Neurotrauma* 15:911–928, 1998.

[27] Mukhin, A. G., S. A. Ivanova, S. M. Knoblach, and A. I. Faden. New in vitro model of traumatic neuronal injury: Evaluation of secondary injury and glutamate receptor-mediated neurotoxicity. *J. Neurotrauma* 14:651–663, 1997.

[28] Newman, E. A., and K. R. Zahs. Calcium waves in retinal glial cells. *Science* 275:844–847, 1997.

[29] Ogden, R. W. Non-Linear Elastic Deformations. Chichester, England: Ellis Harwood, 1984 (Reprinted by Dover Publications Inc., Mineola, NY, 1997). 544

[30] Regan, R. F., and D. W. Choi. The effect of NMDA, AMPA/kainate, and calcium channel antagonists on traumatic cortical neuronal injury in culture. *Brain Res.* 633:236–242, 1994.

[31] Regan, R. F., and S. S. Panter. Traumatic neuronal injury in cortical cell culture is attenuated by 21-aminosteroids. *Brain Res.* 682:144–150, 1995.

[32] Richards, D. A., T. V. Bliss, and C. D. Richards. Differential modulation of NMDA-induced calcium transients by arachidonic acid and nitric oxide in cultured hippocampal neurons. *Eur. J. Neurosci.* 17:2323–2328, 2003.

[33] Rossi, D. J., T. Oshima, and D. Attwell. Glutamate release in severe brain ischaemia is mainly by reversed uptake. *Nature* 403:316–321, 2000.

[34] Ruan, J. S., T. Khalil, and A. I. King. Dynamic response of the human head to impact by three-dimensional finite element analysis. *J. Biomech. Eng.* 116:44–50, 1994.

[35] Rzigalinski, B. A., J. T. Weber, K. A. Willoughby, and E. F. Ellis. Intracellular free calcium dynamics in stretch-injured astrocytes. *J. Neurochem.* 70:2377–2385, 1998.

[36] Saatman, K. E., D. I. Graham, and T. K. McIntosh. The neuronal cytoskeleton is at risk after mild and moderate brain injury. *J. Neurotrauma* 15:1047–1058, 1998.

[37] Smith, D. H., X. H. Chen, J. E. Pierce, J. A. Wolf, J. Q. Trojanowski, D. I. Graham, and T. K. McIntosh. Progressive atrophy and neuron death for one year following brain trauma in the rat. *J. Neurotrauma* 14:715–727, 1997.

[38] Smith, D. H., J. A. Wolf, T. A. Lusardi, V. M. Lee, and D. F. Meaney. High tolerance and delayed elastic response of cultured axons to dynamic stretch injury. *J. Neurosci.* 19:4263–4269, 1999.

[39] Tavalin, S. J., E. F. Ellis, and L. S. Satin. Mechanical perturbation of cultured cortical neurons reveals a stretch-induced delayed depolarization. *J. Neurophysiol.* 74:2767–2773, 1995.

[40] Thompson, D. M., and H. M. Buettner. Schwann cell response to micropatterned laminin surfaces. *Tissue Eng.* 7:247–265, 2001.

[41] Venance, L., N. Stella, J. Glowinski, and C. Giaume. Mechanism involved in initiation and propagation of receptor-induced intercellular calcium signaling in cultured rat astrocytes. *J. Neurosci.* 17:1981–1992, 1997.

[42] Vink, R., T. K. McIntosh, P. Demediuk, M. W. Weiner, and A. I. Faden. Decline in intracellular free Mg^{2+} is associated with irreversible tissue injury after brain trauma. *J. Biol. Chem.* 263:757–761, 1988.

[43] Weber, J. T., B. A. Rzigalinski, and E. F. Ellis. Traumatic injury of cortical neurons causes changes in intracellular calcium stores and capacitative calcium influx. *J. Biol. Chem.* 276:1800–1807, 2001.

[44] Wolf, J. A., P. K. Stys, T. Lusardi, D. Meaney, and D. H. Smith. Traumatic axonal injury induces calcium influx modulated by tetrodotoxin-sensitive sodium channels. *J. Neurosci.* 21:1923–1930, 2001.

[45] Yoon, K. W., H. L. Mitchell, L. D. Broder, R. W. Brooker, and R. K. Delisle. Trauma-induced neurotoxicity in rat hippocampal neurons. *Stroke* 27:122–126, 1996.

[46] Yuan, Q., L. Dougherty, and S. S. Margulies. In vivo human cervical spinal cord deformation and displacement in flexion. *Spine* 23:1677–1683, 1998.

[47] Zhang, L., K. H. Yang, and A. I. King. Comparison of brain responses between frontal and lateral impacts by finite element modeling. *J. Neurotrauma* 18:21–30, 2001.